

PCCP

Accepted Manuscript



This is an *Accepted Manuscript*, which has been through the Royal Society of Chemistry peer review process and has been accepted for publication.

Accepted Manuscripts are published online shortly after acceptance, before technical editing, formatting and proof reading. Using this free service, authors can make their results available to the community, in citable form, before we publish the edited article. We will replace this *Accepted Manuscript* with the edited and formatted *Advance Article* as soon as it is available.

You can find more information about *Accepted Manuscripts* in the [Information for Authors](#).

Please note that technical editing may introduce minor changes to the text and/or graphics, which may alter content. The journal's standard [Terms & Conditions](#) and the [Ethical guidelines](#) still apply. In no event shall the Royal Society of Chemistry be held responsible for any errors or omissions in this *Accepted Manuscript* or any consequences arising from the use of any information it contains.



Journal Name

ARTICLE

Resonant Raman scattering of $\text{ZnS}_x\text{Se}_{1-x}$ solid solutions: role of S and Se electronic states

M. Dimitrievska^a, H. Xie^a, A. J. Jackson^b, X. Fontané^a, M. Espíndola-Rodríguez^a, E. Saucedo^a, A. Pérez-Rodríguez^{a,c}, A. Walsh^b and V. Izquierdo-Roca^a

Received 00th January 20xx,
Accepted 00th January 20xx

DOI: 10.1039/x0xx00000x

www.rsc.org/

A comprehensive Raman resonance scattering study of $\text{ZnS}_x\text{Se}_{1-x}$ (ZnSSe) solid solutions over the whole compositional range ($0 \leq x \leq 1$) has been made using 325 and 455 nm excitation wavelengths. The Raman scattering intensities of the LO ZnS-like and ZnSe-like phonon modes, corresponding to pure S and Se vibrations, respectively, are revealed to be significantly enhanced when excited with 325 nm excitation in the case of S vibrations, and with 455 nm in the case of the Se vibrations. This behavior is explained with the interaction of the excitation photons with the corresponding S or Se electronic states in the conduction band, and further confirmed with first principle simulations. These findings advance the fundamental understanding of the coupling between the electronic transitions and photons in the case of Raman resonance effects, and provide inputs for further studies of lattice dynamics, especially in the case of chalcogenide materials. Additionally, the coexistence of modes corresponding to only S vibrations and only Se vibrations in the ZnSSe alloys makes these results applicable for the compositional assessment of ZnSSe compounds.

Introduction

Wide band gap II-IV semiconductor binaries and their solid solutions have gained considerable attention due to their potential application in electronic and optoelectronic devices. The efficient miscibility of the ZnS and ZnSe compounds in the $\text{ZnS}_x\text{Se}_{1-x}$ (ZnSSe) solid solutions over the whole compositional range, $0 \leq x \leq 1$, enables easy tuning of the band gap energies (ranging from 2.67 eV (ZnSe) to 3.66 eV (ZnS)) and the lattice constants, which additionally enhances the potential application of these materials. ZnSSe compounds have been reported as highly suitable and promising materials for blue lasers, light emitting diodes, light emitters, and wavelength tunable UV photo detectors, due to their wide direct band gap and high photoresistivity.^{1–4} Polycrystalline ZnSSe compounds are excellent candidates for window and/or buffer layers in thin film hetero-junction solar cells and promising alternatives to the presently explored materials such as CdS, which contain toxic Cd.^{5,6} Additionally, because of its low absorption at infrared wavelength and exciton binding energy, ZnSSe is considered as future material in the production of biomedical labels, output couplers, lenses, and optically controlled switches. Changing the ratio of S to Se of ZnSSe compounds leads to tuning of the electron affinity and electrical properties which greatly enhances the blue response of the material.⁷

ZnSSe may also appear as a secondary phase in other multinary compounds, like $\text{Cu}_2\text{ZnSn}(\text{S},\text{Se})_4$, which have shown promising results for application as a thin film absorber layers in solar cells.^{8,9} It has been shown that ZnSSe secondary phases, besides having unfavorable effects on the conversion efficiency of solar cells, are also quite challenging for detection with standard characterization techniques such as X-ray diffraction (XRD). For all these reasons, synthesis and characterization of ZnSSe materials is a very attractive topic. Until now, a wide range of characterization studies of the ZnSSe thin films have been reported, including structural, electrical and optical properties variations in dependence of the S/Se ratio.^{2,5,7,10–16} Raman spectroscopy as such has been extensively used for investigating the lattice vibration dynamics in these systems.^{12,14,17,18} Raman scattering is a powerful non-destructive method which can provide useful information on the structure, morphology and chemical composition of semiconductor materials, as well as on the photon–electron and electron–phonon interactions occurring in these materials. Although many studies have been devoted to compositional dependence of the optical modes in the ZnSSe systems, most are usually done using standard non-resonant Raman conditions. The main disadvantage of the standard excitation methods is the observation of high number of Raman modes with relatively low intensity, which leads to difficulties in the determination of peak positions and phase identification. This is due to very weak Raman scattering efficiency of ZnSSe compounds caused by weak photon–matter interaction under standard excitations (514 and 532 nm lasers).^{19,20} In contrast, resonance Raman methods allow measuring spectra, which are simpler in the sense that the

^a Catalonia Institute for Energy Research (IREC), Jardins de les Dones de Negre 1, 08930 Sant Adrià de Besòs, Spain.

^b Centre for Sustainable Chemical Technologies and Department of Chemistry, University of Bath, Claverton Down, Bath BA2 7AY, United Kingdom.

^c IN²UB, University of Barcelona, C. Martí Franquès 1, 08028 Barcelona, Spain

number of observed independent modes is lower and at the same time, with several orders of magnitude higher intensity.^{20–22} This allows easier identification of the modes and facilitates their correlation with other properties, such as composition, impurities, defects, crystallinity, and electronic band structure. Additionally, use of resonant Raman conditions allows the use of shorter integration times, usually of the order of seconds, which is a significant advantage when compared to other characterization methods, especially in the case of nanosystems, where normally long integration times are required for the structural and electrical characterization. In this work a study of vibrational properties of ZnSSe solid solutions, over the full range of anion compositions, $0 \leq [S]/([S]+[Se]) \leq 1$, was made using resonant Raman spectroscopy. Special focus is put on the changes in the integral intensity of the Raman modes sensitive to anion vibrations, with the variations in the excitation energy. It is observed that Raman modes corresponding to S vibrations are exhibiting resonant behavior in the case of 325 nm excitation, while Raman modes corresponding to Se vibrations become resonant when probed with 455 nm excitation. This behavior is explained by interaction of the excitation photons with the corresponding S or Se states in the electronic band structure, and confirmed by first principles calculations. The understanding of this kind of resonance effects could improve fundamental knowledge not only of the ZnSSe compounds, but also other types of mixed chalcogenide materials, including Cd-(S,Se) and Mo-(S,Se)₂. Finally, these results can be applied for the development of a simple and non-destructive optical methodology for the quantitative measurement of $[S]/([S]+[Se])$ anion composition in ZnSSe solid solutions by means of Raman spectroscopy.

Experimental

Thin film formation

Zn precursors of 80 nm were deposited by DC-magnetron sputtering (Ac450 Alliance Concepts) using a power density of 1.27 W/cm² onto glass substrates. Binary ZnS thin films were produced by reactive annealing of the Zn precursors under sulfur atmosphere at 550 °C, 1bar Ar pressure for 30 min, and using one crucible with 50 mg of sulfur powder (Alfa-Aesar, 99.995%). ZnSe thin films were produced by reactive annealing under selenium atmosphere at 550 °C for 30 min with the flow of Ar to maintain a pressure of 1 mbar, and with one crucible containing 50 mg of selenium powder (Alfa-Aesar, 99.999%). To form ZnSSe alloy films a single-step sulfo-selenization annealing was used.⁸ The process is similar to that used for the pure ZnS or ZnSe films, but varying the ratio of the mixture of sulfur and selenium while maintaining the total weight of the mixture of 50 mg. Two annealing temperature profiles were employed; “one step profile”: 550°C, 30 min, 1 mbar or 1bar; and “two step profile”: first 200°C in 1mbar atmosphere and then 550°C for 30 min in 1 bar atmosphere, which is proved to be beneficial to obtain various Se-rich thin films. The heating

rate for all thermal treatments was 20 °C/min and the cooling process was allowed to proceed naturally.

Characterization

Raman scattering measurements were performed in back scattering configuration with a LabRam HR800-UV and DXR™xi Raman Imaging Microscope. For the HR800-UV system, gas HeCd laser with wavelength of 325 nm was used for excitation. In this system excitation and light collection were made through an Olympus metallographic microscope with a laser spot diameter of the order of 1-2 μm. To avoid effects in the spectra related to potential microscopic inhomogeneities, the spot was rastered over an area of 30 x 30 μm². Furthermore, the DXR™xi Raman Imaging Microscope system works coupled with a 455 nm laser, with a 1-2 μm diameter spot size on the sample. In all cases, and to avoid the presence of thermal effects in the spectra, the power excitation density on the surface of the samples was around 50 W/cm². Under these experimental measurement conditions no thermal effects are observed in the spectra. This has been corroborated by the analysis of spectra measured with different excitation powers. The first-order Raman spectrum of monocrystalline Si was measured as a reference before and after acquisition of each Raman spectrum, and the spectra were corrected with respect to the Si line at 520 cm⁻¹.

XRD patterns were measured on Siemens D500 diffractometer with Cu-Kα radiation ($\lambda=1.54056 \text{ \AA}$) in $\theta-2\theta$ configuration. Refinements of the lattice constant values were carried out by Le Bail analysis using the FullProf package.²³

The band gap energies were determined from the ultraviolet-visible (UV-Vis) spectra which were obtained using a Perkin Elmer Lambda 950 UV/VIS spectrometer.

The composition of the samples was measured using X-ray fluorescence (XRF) spectroscopy performed on the Fisherscope XVD system.

The synthesized films have been imaged by scanning electron microscopy (SEM) using a ZEISS Series Auriga microscope with 5 kV acceleration voltage.

Theoretical calculations

Electronic structure calculations within density functional theory (DFT) were carried out within periodic boundary conditions as implemented in VASP, a quantum chemistry package using plane-wave basis sets.²⁴ 8-atom unit cells were formed for ZnS, a ZnSSe alloy with 3:1 S:Se ratio, and ZnSe (Figure 1). The alloy cell of composition Zn₄S₃Se, provides a mixture of Zn-S and Zn-Se interactions for comparison with the binary compounds; however, the effects of long-range disorder are neglected in this work. The initial lattice parameters were $a = 5.383 \text{ \AA}$ for ZnS and the alloy cell, and $a = 5.667 \text{ \AA}$ for ZnSe, based on crystallographic studies;^{25,26} these structures were optimized with the PBEsol exchange-correlation functional, using projector-augmented wave (PAW) pseudopotentials optimized for the PBE functional and including the Zn 3d states as valence electrons. The basis-set energy cutoff was 500 eV the Brillouin zone was sampled with

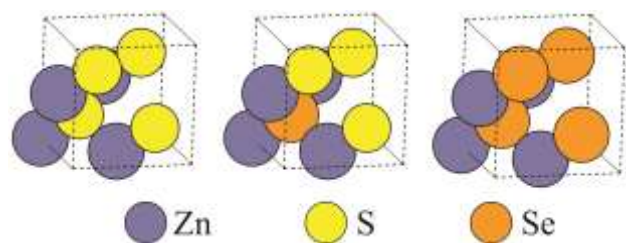


Figure 1. Unit cells for theoretical calculations. Zn (indigo), S (yellow) and Se (orange) atoms in 8-atom ZnS ($a = 5.363 \text{ \AA}$), alloy ($a = 5.431 \text{ \AA}$) and ZnSe ($a = 5.642 \text{ \AA}$) unit cells.

a $5 \times 5 \times 5$ Γ -centered \mathbf{k} -point grid (reduced by symmetry to 10 irreducible points).²⁷ The ionic positions and lattice parameters were optimized by a succession of conjugate gradient procedures until the difference in total energy between relaxation steps was reduced to below 1 meV. The structures optimized with PBEsol were then used for electronic structure calculations with the non-local screened hybrid HSE06 exchange-correlation functional²⁸. The same pseudopotentials and energy cutoff were used for these calculations, while the \mathbf{k} -point mesh density was increased to $15 \times 15 \times 15$ (reduced by symmetry to 120 points). In these cases the initial electronic structure convergence was achieved with Gaussian smearing ($\sigma = 0.05 \text{ eV}$), and the density of states refined by further SCF iterations using the tetrahedron method with Blöchl corrections.

Results and discussion

The crystal structure of ZnSSe solid solutions was characterized by XRD measurements from which representative patterns are presented in Figure 2(a). All main diffraction peaks have been identified to the zinc-blende structure,²⁹ and no evidence of any other phases or impurities have been found. Furthermore, presence of a single and symmetric (111) diffraction peak in all measured patterns implies that all samples are homogeneously alloyed rather than a mixture of ZnS and ZnSe phases. The systematic shift in peak positions toward higher angles as $[S]/([S]+[Se])$ ratio increases correlates with the replacement of smaller S atoms with larger Se atoms, which in turn leads to a decrease in the lattice constants. The lattice constants of the ZnSSe solid solutions were obtained as result of the Le Bail analysis, for which zinc-blende structure was used as a starting model for the refinements. By assuming the validity of Vegard's law and using the lattice constants calculated from the XRD data, the anion compositions $[S]/([S]+[Se])$ of the ZnSSe thin films were determined and presented in Figure 2(b). The obtained results are in agreement with the previously reported data.^{13,30–32}

The band gap energies of the ZnSSe compounds have been evaluated from the UV-vis absorption spectra using the Tauc relation:³³

$$(\alpha h\nu)^n = C(E - E_g) \quad (1)$$

where α is the absorption coefficient, h is the Planck's constant, ν is frequency, $n=2$ for a direct band gap semiconductor material (such as ZnSSe), C is a proportionality constant, E is energy (equal to $h\nu$), and E_g is the band gap energy. The estimated band gap energies for each anion composition of the ZnSSe alloys are shown in Figure 2(b). It is observed that the band gap energies can be tuned from 3.66 eV in pure ZnS thin films to 2.67 eV in pure ZnSe thin films, just by changing the anion composition in the samples. The change in the band gap energies with the anion composition $x = [S]/([S] + [Se])$ shows nonlinear behavior and can be fitted as a quadratic function of x :

$$E_g(x) = xE_g(\text{ZnS}) + (1-x)E_g(\text{ZnSe}) - x(1-x)b \quad (2)$$

where $E_g(\text{ZnSe})$, $E_g(\text{ZnS})$, and $E_g(x)$ are the band gap energies of ZnSe, ZnS, and their alloy, respectively, while b is the bowing constant, and in this case the best fit was obtained for $b = 0.70(6)$, which is in agreement with previously reported values.³⁴

The Raman scattering spectra of ZnSSe solid solutions measured under ultra-violet (UV) ($\lambda = 325 \text{ nm}$, 3.82 eV) and blue ($\lambda = 455 \text{ nm}$, 2.72 eV) excitations are shown in Figures 3. Raman spectra of the pure ZnS measured under resonant conditions (UV excitation) is characterized by the strongly enhanced longitudinal optical (LO) phonon mode observed at 348 cm^{-1} .²⁰ This mode is attributed to vibrations of only S anions in the lattice. An illustration of the normal displacements of the LO phonon mode, obtained from the first principles simulations is presented in the inset of Figure 3(a). Second (LO2) and third (LO3) orders of this mode are also observed at 696 and 1044 cm^{-1} frequencies, respectively. Additionally, a lower intensity peak is observed at 277 cm^{-1} , and attributed to the fundamental transverse optical (TO) phonon mode. Bands at 419, 635 and 978 cm^{-1} are attributed to the higher order combination bands of the fundamental modes.³⁵ In the case of pure ZnSe, a resonant Raman spectrum is measured under the blue excitation, and characterized by the strongly enhanced LO mode at 250 cm^{-1} , attributed to vibrations of only Se anions, and a low intensity TO mode observed at 205 cm^{-1} .³⁶ Again, second (LO2) and third (LO3) order peaks are observed at 501 and 752 cm^{-1} , respectively. The first order Raman spectra of ZnSSe solid solutions are characterized by the presence of two dominant peaks in the frequency region $270 - 350 \text{ cm}^{-1}$, and two dominant peaks in the frequency region $200 - 270 \text{ cm}^{-1}$. The peaks in the higher frequency region are identified as ZnS-like peaks corresponding to TO and LO phonon modes involving S vibrations, and the peaks in the lower frequency region are identified as ZnSe-like peaks corresponding to TO and LO phonon modes involving Se vibrations.^{37,38} This agrees with the existence of a two-mode behavior for these peaks, as previously reported.^{17,37,39,40}

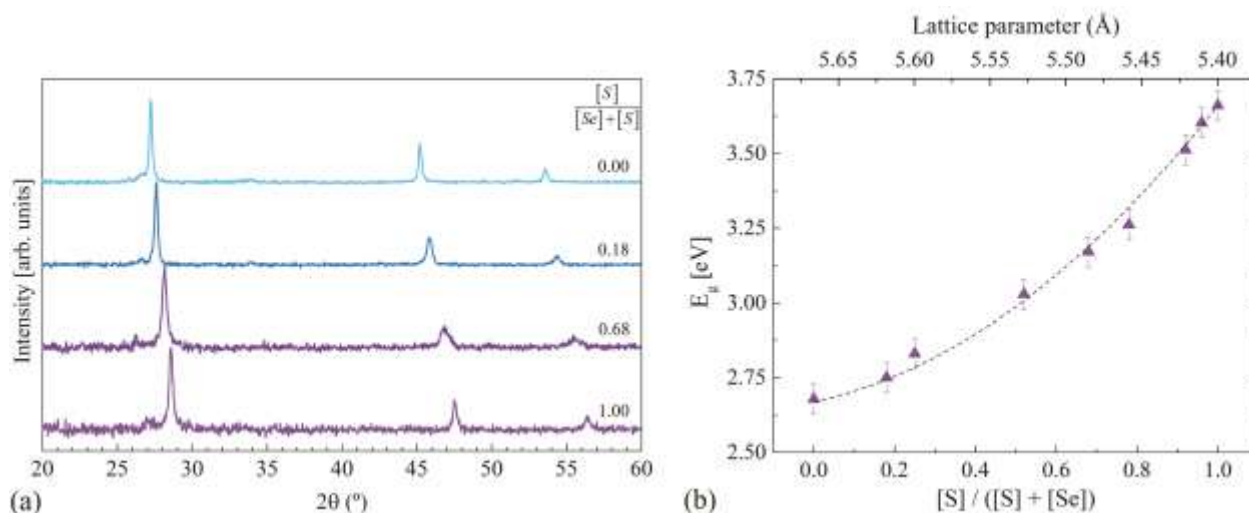


Figure 2. (a) Representative XRD patterns of ZnSSe solid solutions for different anion compositions (b) Band gap energies in dependence of $[S] / ([S] + [Se])$ compositions and lattice constants

The optical phonon frequencies vary with the changes in composition. With the increase in S composition, the LO ZnSe-like peak shifts downward in frequency, while the TO ZnSe-like peak monotonically moves upward. For the very S-rich samples, these two modes almost overlap, and then finally disappear for $x = 1$. Similar behavior is observed for the LO and TO ZnS-like peaks with the increase in the Se composition. The compositional dependence of LO and TO frequencies for both ZnS-like and ZnSe-like peaks are shown in Figure 4. Solid lines in Figure 4 present the calculated phonon frequencies of the modes using the modified-random-element-isodisplacement (MREI) model.¹⁷ Additional information about the MREI model, as well as the explanation of the calculation process and the parameter values used for obtaining results presented in Figure 4, is given in Ref. [17]. The experimental data presented in Figure 4 is in good agreement with the model predictions and as well as previously reported results.^{39,40}

Asymmetrical broadening in the low frequency side of the LO ZnS-like peak can be observed with the decrease in the S composition in the Raman spectra measured with 325 nm excitation. Similarly, asymmetrical broadening in a low frequency side of the LO ZnSe-like peak is noticeable in the Raman spectra measured with 455 nm excitation, with the decrease in Se composition. This phenomenon is attributed to the phonon confinement effects arising from the loss of translational symmetry in the crystal caused by the alloy disorder.³⁹⁻⁴¹

An interesting phenomena which was not previously observed in the ZnSSe systems, is the intensity dependence of the LO ZnS-like and LO ZnSe-like modes with the excitation energy. Figures 5 (a) and (b) present the changes in the intensity of the LO ZnS-like and ZnSe-like modes with respect to the difference between the energy band gap and the excitation energy.

Three kinds of resonance behavior can be observed from the results presented in Figure 5. In case of S-rich ZnSSe samples, only LO ZnS-like peaks are enhanced when measured with UV excitation; while LO ZnSe-like peaks do not exhibit resonance behavior for any of the used excitation wavelengths. A reverse

situation is observed for the Se-rich ZnSSe samples, where LO ZnSe-like peaks are enhanced in the Raman spectra measured with blue excitation; while LO ZnS-like peaks show non-resonance behavior for any of the used excitation wavelengths. Lastly, for the case of intermediate anion compositions, the LO ZnS-like peaks become resonant when using the UV excitation and the LO ZnSe-like peaks become resonant when probed the blue excitation.

According to these experimental results, UV excitation only enhances modes correlated to vibrations of S anions, while blue excitation only induces resonance effects in modes attributed to vibrations of Se anions. This behavior suggests that UV photons mostly interact with S electronic states, while blue photons interact with Se states. Further explanation of these results can be made by taking in account the electronic band structure of ZnSSe compounds and working principles of the resonance Raman effect.

In general, Raman scattering intensity can be defined as:^{42,43}

$$I(\omega_i) \propto \omega_s^4 |\hat{e}_s \cdot R \cdot \hat{e}_i|^2 \left| \sum_{\alpha\beta} \frac{1}{(E_\alpha - \hbar\omega_i - i\Gamma_\alpha)(E_\beta - \hbar\omega_s - i\Gamma_\beta)} \right|^2 \quad (3)$$

where ω_s and ω_i are the scattered and the incoming photon frequencies, respectively; E_α and E_β are the energies of the intermediate crystal states, R is the Raman tensor, \hat{e}_s and \hat{e}_i are the scattered and the incident polarization vectors, and Γ_α and Γ_β are damping constants. The first term in the Eq. 3 represents the dipole transition radiation; the second term represents the Raman selection rules, which is dependent on the crystal symmetry, while the last term leads to the resonance effects. As the incident excitation energy is tuned to the energy of the intermediate state, the denominator in Eq. 3 becomes smaller, which then leads to the enhancement in the Raman intensity, and thus the resonance effects. Raman resonance effects in semiconductors may be achieved if the excitation energy approaches the band-gap energy, or via the interaction of the incident photon with the exciton states or the impurity states.

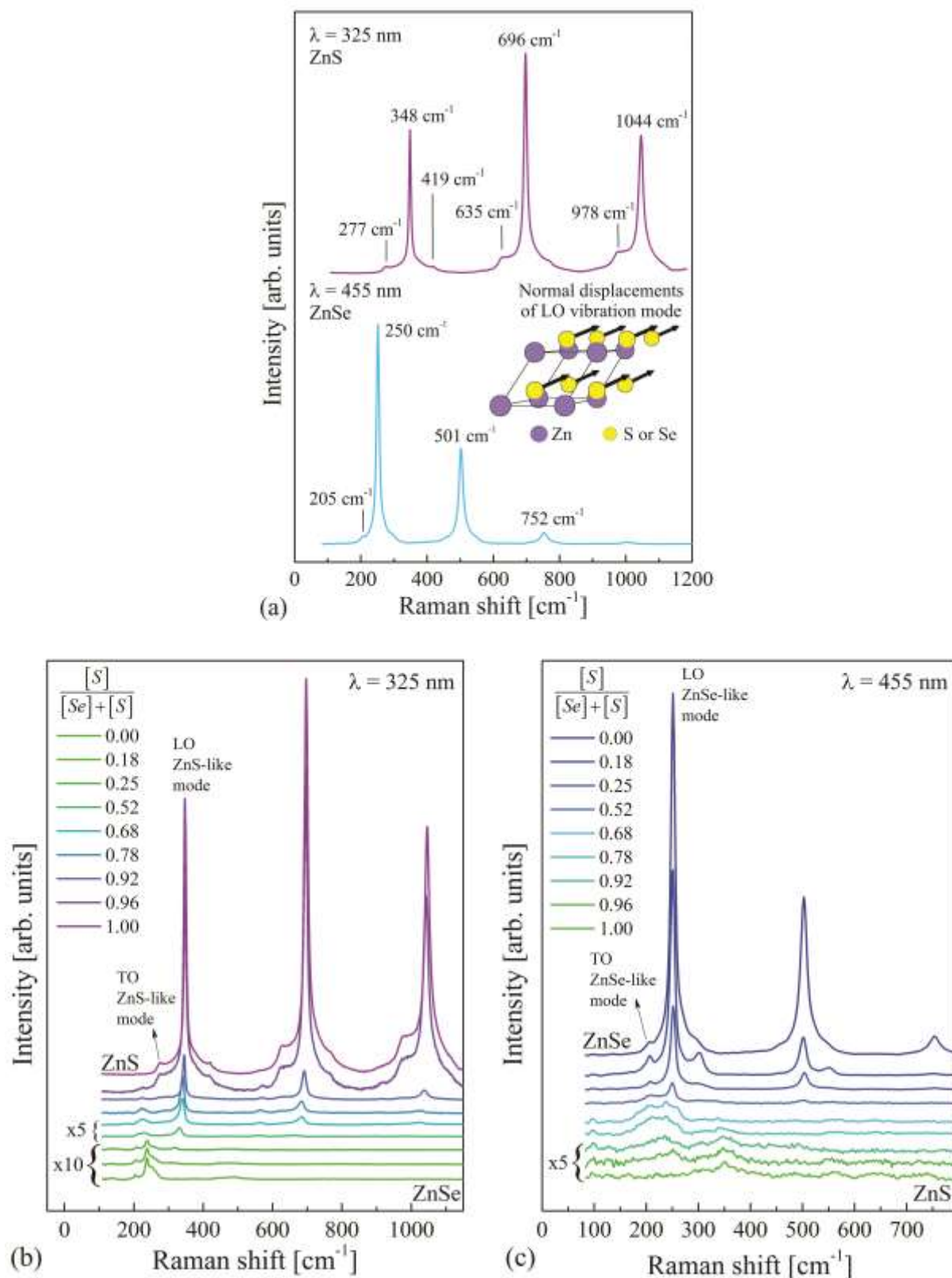


Figure 3. (a) Normalized reference Raman spectra of pure ZnS and ZnSe compounds with the identification of modes measured under resonant conditions; Inset shows the normal displacements of the LO phonon mode for pure ZnS or ZnSe, with arrows indicating the direction of the movement of the atoms; (b) and (c) Raman spectra of ZnS_xSe_{1-x} solid solutions measured with 325 and 455 nm excitation wavelengths. Some of the low intensity spectra in both cases were multiplied $\times 5$ or $\times 10$ for more details, as labeled in the figure.

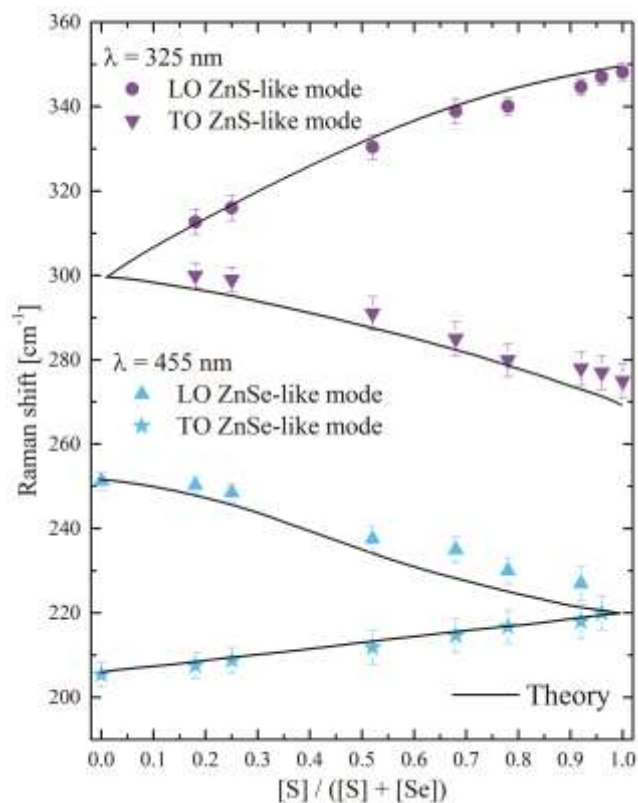


Figure 4. The optical phonon frequencies of the ZnSe-like and ZnS-like modes as a function of the anion composition $[S]/([S] + [\text{Se}])$. The ZnSe-like and ZnS-like mode frequencies were determined from the resonant Raman spectra measured with 455 and 325 nm excitation wavelength, respectively. The solid lines represent the theoretical frequencies obtained by the modified random-element-isodisplacement model.

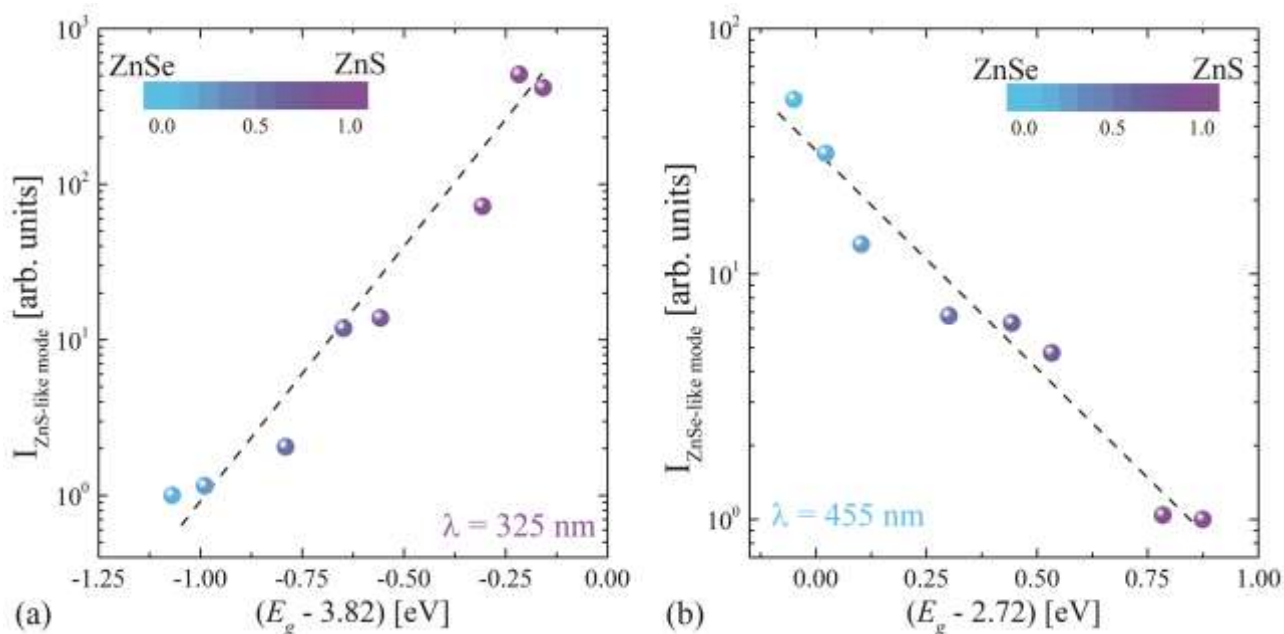


Figure 5. Enhancement in the intensity of the (a) LO ZnS-like mode and (b) LO ZnSe-like mode in dependence of the difference between the band gap energy of the ZnSSe thin films and the excitation energy. Dashed lines are eye guides.

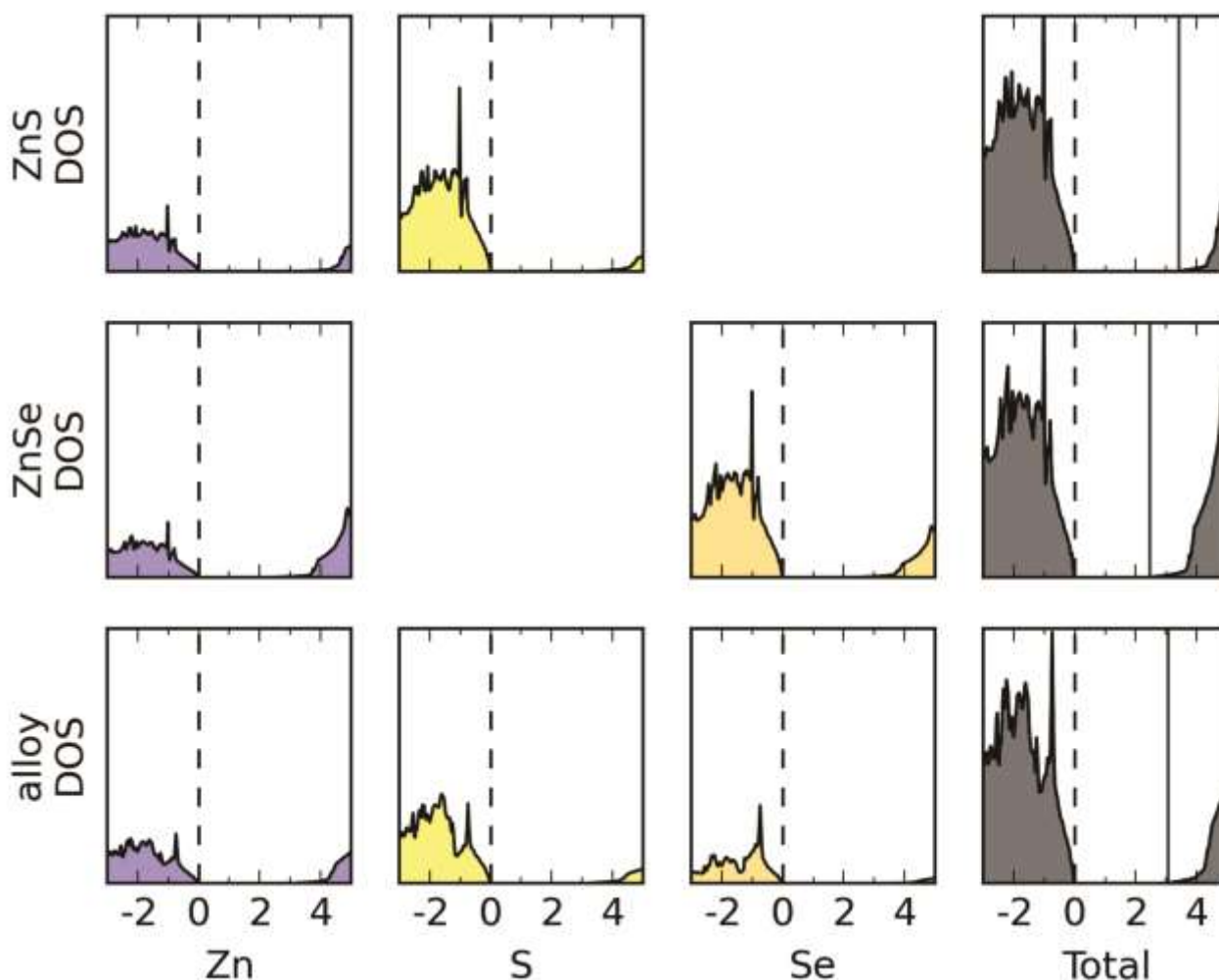


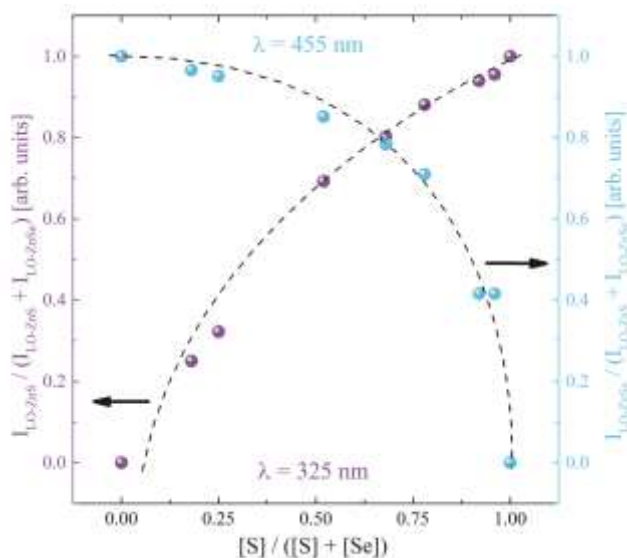
Figure 6. Partial and total density of states (DOS) for ZnS, ZnSe and $\text{ZnS}_{0.75}\text{Se}_{0.25}$ alloy obtained from hybrid DFT calculations. Horizontal axes give energy relative to the Fermi level (indicated with a dashed line) in eV. Right-most column is total DOS; vertical solid line indicates the conduction band minimum (CBM).

For crystals with intermediate composition, changes in the S and Se electronic states are low enough to allow the preservation of the resonant excitation behavior of the LO ZnS-like and ZnSe-like modes with the UV and blue excitations, respectively. However, for S-rich or Se-rich alloys this is not the case. As example of the last situation, figure 6 shows the full and species-projected density of states for ZnS, $\text{ZnS}_{0.75}\text{Se}_{0.25}$ and ZnSe. As can be seen in the case of $\text{ZnS}_{0.75}\text{Se}_{0.25}$, the above-gap S states are shifted slightly closer to the Fermi level in comparison to the pure ZnS compound, while the above-gap Se states are shifted considerably further from the Fermi level relative to the pure ZnSe compound.

This means that for S-rich ZnSe samples, interaction between S states and UV photons is expected, due to their similar energies, while no interaction will occur between Se states and blue photons, because of their energy mismatch. This should then lead to resonance behavior of the LO ZnS-like modes, when probed with UV excitation, and non-resonance behavior

of LO ZnSe-like modes when probed with blue excitation, which is experimentally observed. Opposite situation is expected in the case of Se-rich samples. Similar resonance effects were also observed in the case of kesterite solid solutions $\text{Cu}_2\text{ZnSn}_x\text{Se}_{1-x}$.⁴⁷

Finally, these results can be applied for the development of a simple and non-destructive optical methodology for the quantitative measurement of $[\text{S}]/([\text{S}]+[\text{Se}])$ anion composition in ZnSSe solid solutions by means of Raman spectroscopy, similarly to the study presented in [48]. Since intensity of LO ZnS-like and ZnSe-like modes is proportional to the concentration of S and Se in the material, respectively, then plotting the integral intensity ratio of these two bands versus the anion composition should give the calibration curves which can be later used for the estimation of anion composition in unknown ZnSSe samples. An example of this kind of plot is given in Figure 7. As shown in the figure, for S-poor compositions changes in the relative intensity of the ZnS-like



peak are very sensitive to changes in the alloy composition, while for S-rich compositions changes in the relative intensity Figure 7. Anion composition in dependence of integral intensity ratio of LO ZnS-like and LO ZnSe-like peaks calculated from Raman spectra measured with 325 and 455 nm excitation.

of the ZnSe-like peak are very sensitive to changes in the alloy composition. In general, this methodology is completely independent of the experimental conditions of the measurements and of the type of samples, which is another advantage of using Raman spectroscopy for the estimation of the anion composition in this kind of materials.

Conclusions

This work describes joint experimental and theoretical investigation of the Raman resonance effects in ZnSSe solid solutions. Resonance behavior is observed in the Raman modes corresponding to the anion vibrations, when changing the excitation energy from UV (325 nm) to blue (455 nm). Significant enhancement in the Raman intensity of the LO ZnS-like modes, corresponding to pure S vibrations, is observed in cases of S-rich and intermediate compositions when excited with UV energy. On the other side, LO ZnSe-like modes attributed to pure Se vibrations, are enhanced in the case of blue excitation for samples with Se-rich and intermediate compositions. This enhancement of only certain Raman modes in the spectra is explained by interaction of the excitation photon with the corresponding S or Se states in the electronic band structure, and confirmed by the first principle calculations. Raman resonant effects in this case are achieved due to the tuning of the excitation energy with the energy of the S or Se electronic states in the conduction band. These findings advance the fundamental understanding of the coupling between the electronic transitions and photons in the case of Raman resonance effects, and provide inputs for further studies of lattice dynamics, especially in the case of

chalcogenide materials. Additionally, application of Raman resonant conditions in the case of this kind of materials can be used for developing simple and non-destructive optical methodology for the quantitative measurement of $[S]/([S]+[Se])$ anion composition. They should also enable easier characterization of the ZnSSe system, like reducing the integration time of the Raman measurements, which is extremely important in the case of nanosystems.

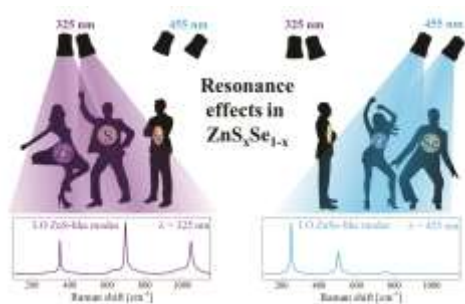
Acknowledgements

The research leading to these results has received funding from the People Program (Marie Curie Actions) of the European Union's Seventh Framework Program FP7/2007-2013/ under REA grant agreement n°316488 (KESTCELLS). Authors from IREC and IN²UB belong to the M-2E (Electronic Materials for Energy) Consolidated Research Group and the XaRMAE Network of Excellence on Materials for Energy of the "Generalitat de Catalunya". E.S. thanks the Government of Spain for the "Ramon y Cajal" fellowship (RYC-2011-09212) and H. X. thanks support from the "China Scholarship Council" fellowship (CSC N° 201206340113). A.J.J. is funded by the EPSRC Doctoral Training Centre in Sustainable Chemical Technologies (EP/G03768X/1). A.W. acknowledges support from the Royal Society and the ERC (grant no. 277757). DFT calculations made use of UK national facility ARCHER, via A.J.J. and A.W.'s membership of the UK's HPC Materials Chemistry Consortium which is funded by EPSRC grant EP/L000202, and of the University of Bath's HPC facilities.

References

- 1 D. S. Patil and D. K. Gautam, *Phys. B Condens. Matter*, 2004, **344**, 140–146.
- 2 S. A.-B. Nasrallah, S. B. Afia, H. Belmabrouk and M. Said, *Eur. Phys. J. B - Condens. Matter Complex Syst.*, 2005, **43**, 3–9.
- 3 Y. Ichimura, K. Kishino, M. Satake, M. Kuramoto and A. Yoshida, *J. Cryst. Growth*, 1995, **150**, Part 2, 812–816.
- 4 H. Okuyama, E. Kato, S. Itoh, N. Nakayama, T. Ohata and A. Ishibashi, *Appl. Phys. Lett.*, 1995, **66**, 656–658.
- 5 Y. P. V. Subbaiah, P. Prathap, K. T. R. Reddy, D. Mangalaraj, K. Kim and J. Yi, *J. Phys. Appl. Phys.*, 2007, **40**, 3683.
- 6 S. V. Sorokin, S. V. Gronin, E. A. Evropeytsev, I. V. Sedova, A. A. Toropov and S. V. Ivanov, *J. Cryst. Growth*.
- 7 S. Fridjine, S. Touihri, K. Boubaker and M. Amlouk, *J. Cryst. Growth*, 2010, **312**, 202–208.
- 8 H. Xie, M. Dimitrievska, X. Fontané, Y. Sánchez, S. López-Marino, V. Izquierdo-Roca, V. Bermúdez, A. Pérez-Rodríguez and E. Saucedo, *Sol. Energy Mater. Sol. Cells*, 2015, **140**, 289–298.
- 9 A. Fairbrother, L. Fourdrinier, X. Fontané, V. Izquierdo-Roca, M. Dimitrievska, A. Pérez-Rodríguez and E. Saucedo, *J. Phys. Chem. C*, 2014, **118**, 17291–17298.
- 10 P. Kannappan, K. Asokan, J. B. M. Krishna and R. Dhanasekaran, *J. Alloys Compd.*, 2013, **580**, 284–289.
- 11 P. Kannappan and R. Dhanasekaran, *J. Cryst. Growth*, 2014, **401**, 691–696.
- 12 L.-J. Chen, C.-R. Lee, Y.-J. Chuang, Z.-H. Wu and C. Chen, *CrystEngComm*, 2015, **17**, 4434–4438.

- 13 R. G. Valeev, E. A. Romanov, V. L. Vorobiev, V. V. Mukhgalin, V. V. Kriventsov, A. I. Chukavin and B. V. Robouch, *Mater. Res. Express*, 2015, **2**, 025006.
- 14 T. Basak, M. N. Rao, S. L. Chaplot, N. Salke, R. Rao, R. Dhanasekaran, A. K. Rajarajan, S. Rols, R. Mittal, V. B. Jayakrishnan and P. U. Sastry, *Phys. B Condens. Matter*, 2014, **433**, 149–156.
- 15 G. L. Agawane, S. W. Shin, S. A. Vanalakar, A. V. Moholkar, K. V. Gurav, M. P. Suryawanshi, J. Y. Lee, J. H. Yun and J. H. Kim, *Mater. Res. Bull.*, 2014, **55**, 106–113.
- 16 H. K. Sadekar, A. V. Ghule and R. Sharma, *J. Alloys Compd.*, 2011, **509**, 5525–5531.
- 17 I. F. Chang and S. S. Mitra, *Phys. Rev.*, 1968, **172**, 924–933.
- 18 J. F. Scott, T. C. Damen, W. T. Silfvast, R. C. C. Leite and L. E. Cheesman, *Opt. Commun.*, 1970, **1**, 397–399.
- 19 S. S. Kumar, M. A. Khadar, K. G. M. Nair, S. Dhara and P. Magudapathy, *J. Raman Spectrosc.*, 2008, **39**, 1900–1906.
- 20 A. Fairbrother, V. Izquierdo-Roca, X. Fontané, M. Ibáñez, A. Cabot, E. Saucedo and A. Pérez-Rodríguez, *CrystEngComm*, 2014, **16**, 4120–4125.
- 21 M. Dimitrievska, A. Fairbrother, X. Fontané, T. Jawhari, V. Izquierdo-Roca, E. Saucedo and A. Pérez-Rodríguez, *Appl. Phys. Lett.*, 2014, **104**, 021901.
- 22 M. Placidi, M. Dimitrievska, V. Izquierdo-Roca, X. Fontané, A. Castellanos-Gomez, A. Pérez-Tomás, N. Mestres, M. Espindola-Rodríguez, S. López-Marino, M. Neuschitzer, V. Bermudez, A. Yaremko and A. Pérez-Rodríguez, *2D Mater.*, 2015, **2**, 035006.
- 23 J. Rodríguez-Carvajal, *Phys. B Condens. Matter*, 1993, **192**, 55–69.
- 24 G. Kresse and J. Hafner, *Phys. Rev. B*, 1993, **47**, 558–561.
- 25 J. C. Jamieson and H. H. Demarest Jr., *J. Phys. Chem. Solids*, 1980, **41**, 963–964.
- 26 P. D. O. Madelung, in *Semiconductors: Data Handbook*, Springer Berlin Heidelberg, 2004, pp. 173–244.
- 27 J. P. Perdew, A. Ruzsinszky, G. I. Csonka, O. A. Vydrov, G. E. Scuseria, L. A. Constantin, X. Zhou and K. Burke, *Phys. Rev. Lett.*, 2008, **100**, 136406.
- 28 A. V. Krukau, O. A. Vydrov, A. F. Izmaylov and G. E. Scuseria, *J. Chem. Phys.*, 2006, **125**, 224106.
- 29 J. Baars and G. Brandt, *J. Phys. Chem. Solids*, 1973, **34**, 905–909.
- 30 Y. Matsushima, K. Yoshino, Y. Yamamoto, S. R. Tiong and M. Hiramatsu, *J. Cryst. Growth*, 1992, **117**, 328–330.
- 31 O. Senthil Kumar, S. Soundeswaran and R. Dhanasekaran, *Mater. Chem. Phys.*, 2004, **87**, 75–80.
- 32 O. Senthil Kumar, S. Soundeswaran, D. Kabiraj, D. K. Avasthi and R. Dhanasekaran, *J. Cryst. Growth*, 2005, **275**, e567–e570.
- 33 J. Tauc and A. Menth, *J. Non-Cryst. Solids*, 1972, **8–10**, 569–585.
- 34 S. Park, H. Kim, C. Jin and C. Lee, *Curr. Appl. Phys.*, 2012, **12**, 499–503.
- 35 W. G. Nilsen, *Phys. Rev.*, 1969, **182**, 838–850.
- 36 W. Taylor, *Phys. Lett. A*, 1967, **24**, 556–558.
- 37 E. A. Vinogradov, B. N. Mavrin, N. N. Novikova, V. A. Yakovlev and D. M. Popova, *Laser Phys.*, 2009, **19**, 162–170.
- 38 M. Dimitrievska, A. Fairbrother, E. Saucedo, A. Pérez-Rodríguez and V. Izquierdo-Roca, *Appl. Phys. Lett.*, 2015, **106**, 073903.
- 39 K. Hayashi, N. Sawaki and I. Akasaki, *Jpn. J. Appl. Phys.*, 1991, **30**, 501.
- 40 J. Lu, H. Liu, C. Sun, M. Zheng, M. Nripan, G. S. Chen, G. M. Subodh, X. Zhang and C. H. Sow, *Nanoscale*, 2012, **4**, 976–981.
- 41 M. Dimitrievska, A. Fairbrother, A. Pérez-Rodríguez, E. Saucedo and V. Izquierdo-Roca, *Acta Mater.*, 2014, **70**, 272–280.
- 42 W. H. Weber and R. Merlin, Eds., *Raman Scattering in Materials Science*, Springer Berlin Heidelberg, Berlin, Heidelberg, 2000, vol. 42.
- 43 P. YU and M. Cardona, *Fundamentals of Semiconductors: Physics and Materials Properties*, Springer Science & Business Media, 2010.
- 44 J. E. Bernard and A. Zunger, *Phys. Rev. B*, 1987, **36**, 3199–3228.
- 45 S.-H. Wei and A. Zunger, *J. Appl. Phys.*, 1995, **78**, 3846–3856.
- 46 Y.-H. Li, A. Walsh, S. Chen, W.-J. Yin, J.-H. Yang, J. Li, J. L. F. D. Silva, X. G. Gong and S.-H. Wei, *Appl. Phys. Lett.*, 2009, **94**, 212109.
- 47 M. Dimitrievska, H. Xie, A. Fairbrother, X. Fontané, G. Gurieva, E. Saucedo, A. Pérez-Rodríguez, S. Schorr and V. Izquierdo-Roca, *Appl. Phys. Lett.*, 2014, **105**, 031913.
- 48 M. Dimitrievska, G. Gurieva, H. Xie, A. Carrete, A. Cabot, E. Saucedo, A. Pérez-Rodríguez, S. Schorr and V. Izquierdo-Roca, *J. Alloys Compd.*, 2015, **628**, 464–470.

**Table of content:**

A combined theoretical and experimental study of the enhancement in the Raman mode intensities of ZnS_xSe_{1-x} compounds, under various resonant conditions, is presented, leading to more detailed insights about the role of chalcogen electronic states in the photon-matter interaction.